

Shear strength of a compacted scaly clay in variable saturation conditions

Marco Rosone · Camillo Airò Farulla ·
Alessio Ferrari

Received: 29 November 2013 / Accepted: 20 February 2015 / Published online: 25 March 2015
© Springer-Verlag Berlin Heidelberg 2015

Abstract Scaly clays are stiff and highly fissured clays often used as construction materials. This paper presents the results of triaxial compression tests carried out on saturated and unsaturated samples of a compacted scaly clay. Complementary investigation on the microstructural features and their evolution with the amount of water stored into the material are also presented in order to shed light on the evolution of the micro- and macroporosity with suction. The water retention behaviour of the compacted scaly clay is also addressed. The results from the controlled suction triaxial tests are used to discuss the applicability of a single-shear strength criterion to compacted double-structured clays when the effective stress concept for unsaturated soils is used. The choice of the degree of saturation to be included in the effective stress definition for obtaining a satisfactory representation of the shear strength is addressed. It is shown that the best results are obtained when the macropore degree of saturation is considered along with its evolution during the applied stress path.

Keywords Compacted clay · Effective stress · Microstructure · Scaly clay · Shear strength · Suction · Unsaturated soils

1 Introduction

Scaly clays are stiff tectonized clays widespread in Sicily and South Italy. Due to their complex geological history, they are strongly over-consolidated and highly fissured. A thick network of discontinuities subdivides the clays in tightly interlocked small stiff clayey fragments (scales), almost always angular, whose size ranges from a few millimetres to several centimetres. This peculiar structural pattern greatly controls the mechanical behaviour of the material. Scaly clays also have received significant interest as construction materials, since their structural characteristics and natural water content allow their compaction as excavated, in order to obtain a material with low permeability and appreciable shear strength and stiffness, suitable for the realization of dam cores and waste confinement liners.

Intense research work has been carried out to analyse the structural features and hydro-mechanical behaviour of natural and compacted scaly clays. Airò Farulla and Nocilla [5] analysed the effects of the discontinuities on the shear strength of undisturbed samples by means of direct shear tests; the study pointed out the strong influence on the strength of the orientation of the discontinuities with respect to the imposed failure surface. Airò Farulla and Valore [8] studied the shear strength of compacted scaly clay samples collected from different sites showing that the scales survive the compaction process although their size decreases and they still govern the shear strength behaviour of the material. Picarelli et al. [23], analysing geotechnical

M. Rosone · C. Airò Farulla
Dipartimento di Ingegneria Civile, Ambientale, Aerospaziale,
dei Materiali (DICAM), Università degli Studi di Palermo,
Viale delle Scienze Ed. 8, 90128 Palermo, Italy
e-mail: marco.rosone@unipa.it

C. Airò Farulla
e-mail: camillo.airofarulla@unipa.it

A. Ferrari (✉)
Laboratory for Soil Mechanics (LMS), School of Architecture,
Civil and Environmental Engineering (ENAC), Ecole
Polytechnique Fédérale de Lausanne (EPFL), Station 18,
1015 Lausanne, Switzerland
e-mail: alessio.ferrari@epfl.ch

works involving tectonized stiff clay outcropping along the Italian Apennines, pointed out how their mechanical behaviour is strongly governed by fabric, structural and physico-chemical environmental conditions. Vitone et al. [31] investigated the mechanical behaviour of the natural clays in the light of their different fissuring features and underlined that for clays of fissuring intensity from high to very high, structure is detrimental to strength so that undisturbed fissured clay strength is even lower than that of reconstituted clay.

Scaly clays compacted on the dry state of optimum present some typical features of double-structured clayey materials [19, 22, 29]. A comprehensive microstructural investigation campaign has been carried out to provide a better insight into the fabric features of scaly clay and its evolution during the compaction and saturation phase [3, 4, 7]. The as-compacted state always presents a clear double porosity arrangement, where the micropores are related to the pores within the clay assemblages (composed of scaly fragments and clay aggregates formed during sample preparation), while macropores refer to the pore network between the assemblages. Hydro-mechanical processes have strong effects on this structural arrangement. Upon suction cycling, the assemblages and then the micropores present a reversible volume change behaviour, while the macropores evolve in an irreversible manner during the first cycles and attain a reversible behaviour after three to four cycles. In particular, it has been observed that upon saturation, assemblages swell invading macropores so that a monomodal pore diameter distribution is obtained. During compaction, macropores are reduced strongly as compaction energy increases, while micropores are not influenced and their initial distribution within the assemblages is preserved.

The microstructural features and their evolutions have a strong impact on the volumetric and retention behaviour of compacted scaly clays. The swelling/shrinkage response of the material upon suction variations is a consequence of the evolution of the different structural levels; in particular, the material can undergo cumulative swelling or settlement depending on stress level [2, 3] and the over-consolidation condition [14]. Retention curves are strongly influenced by the void ratio in terms of air entry value and hysteresis domain [1].

For saturated samples, the effects of the presence of the scaly fragments have been discussed by Airò Farulla and Rosone [6], showing that even after saturation the scales are still present as discernible units and they govern the overall strength of the material.

Limited evidence is available for the shear strength in unsaturated conditions. A deep understanding on the effects of suction on the shear strength of the material is a fundamental requirement in order to predict the stability of

the constructions. It should be considered that the scaly clays are compacted in an unsaturated state and will be subjected to variations in the degree of saturation of different intensities depending on the environmental boundary conditions.

With regard to this topic, the paper presents a comprehensive assessment of the shear strength of compacted scaly clay in unsaturated conditions. Controlled suction triaxial tests were run with the aim to quantify the suction contribution to the shear strength. Complementary microstructural studies and some peculiar aspects of the water retention behaviour are presented initially in order to shed light on the effects of the double-structural features of the material on the strength in unsaturated conditions. An insight into the evolution of the microstructure with the amount of water stored into the material is provided. Finally, the choice of the shear strength parameters is discussed considering the effective stress definition for unsaturated soils.

2 Tested material

Tested samples were prepared using a stiff and highly fissured clay outcropping near Palermo (Sicily), used for core construction in two earth dams. The tested material is a silty clay having liquid and plastic limits within the range of $w_l = 60\text{--}64\%$, $w_p = 20\text{--}26\%$, mean specific gravity $G_s = 2.76$ and natural water content $w_n = 20\%$.

The material was excavated at depth of 3–4 m from soil surface and air-dried at laboratory conditions (temperature $T = 20\text{ }^\circ\text{C}$ and relative humidity $\text{RH} \approx 45\%$). The dried clay having a hygroscopic water content $w_h \approx 5\%$ was disaggregated by means of a rubber pestle, and the fraction passing through a No. 4 ASTM sieve was selected; this fraction was constituted by scales, fragments of scales and powdered clay. The selected material was moistened to the water content $w = 15\%$ and dynamically compacted to the target dry density $\gamma_d = 17.4\text{ kN/m}^3$. These initial physical characteristics of the specimens were fixed as the mean values of results from control tests on field-compacted scaly clay during construction of the two core earth dams [8]. Dynamic compaction was carried out by means of a modified Harvard apparatus with a cylindrical mould of 76 mm height and 38 mm inner diameter. The adopted procedure made use of five layers (14 tamps per layer) and a tamping force of 275 N, giving optimum values $w_{\text{opt}} = 17\%$, $\gamma_{d,\text{max}} = 17.5\text{ kN/m}^3$. Therefore, all specimens were prepared on the left side of the optimum. The water content and the initial dry density after compaction were in the range of $w = 15 \pm 0.4\%$ and $\gamma_d = 17.4 \pm 0.2\text{ kN/m}^3$. Corresponding initial void ratio, water ratio (ratio of the volume of water to the volume of solid phase,

$e_w = w G_s$) and degree of saturation values were as follows: $e_0 = 0.56 \pm 0.03$, $e_{w0} = 0.41 \pm 0.02$, and $S_{r0} = 0.74 \pm 0.04$ (Table 1). A vertical total stress of about 1 MPa was required to prepare specimens with the similar characteristics by static compaction. Initial total suction of the as-compacted material was measured by means of a dew-point chilled-mirror psychrometer [11, 21] and was approximately 2 MPa; the air entry value for the corresponding void ratio was about 100 kPa [1].

3 Microstructure and water retention features

The hydro-mechanical behaviour of scaly clays is influenced deeply by the fabric arrangement at the microstructural level. With the aim to provide a solid background for the interpretation of the unsaturated scaly clay shear strength data, this section presents results from a complementary investigation programme on the microstructural features of the compacted scaly clay and on their evolution along suction changes. Some peculiar aspects of the water retention behaviour along main wetting and drying paths at constant void ratio values are also outlined.

Microstructural analyses were carried out by combining mercury intrusion porosimetry (MIP) tests and scanning electronic microscope (SEM) observations. MIP tests were

performed using a porosimeter (Pascal 140–240 series, Thermo Scientific Corp.) attaining a maximum intrusion pressure of 200 MPa, which corresponds to an entrance pore diameter of approximately 7 nm. Macropores were detected at the beginning of the tests in the low pressure unit operating between 0 and 400 kPa. The advancing non-wetting contact angle between mercury and the clay minerals was assumed to be 140° [26]. SEM observations were performed on a FEI Quanta 200f microscope. MIP tests and SEM observations were carried out on samples dehydrated by means of a freeze-drying technique consisting in quick freezing the samples by dipping them in liquid nitrogen (boiling temperature -198°C) and sublimation with vacuum pump at -60°C for 24 h.

As-compacted specimens for SEM and MIP tests were prepared by initially moistening the selected air-dried material passing at No. 10 ASTM sieve (mesh aperture of 2 mm) at the target water content and by compacting statically the material in a small rigid cylindrical mould of 9 mm inner diameter and 9.3 mm height. Other specimens were recovered by means of a small cylindrical sampler (inner diameter of 10 mm and height of 10 mm) from samples subjected to different hydro-mechanical stress paths in oedometric tests.

Figure 1 depicts the results from MIP tests in terms of cumulative intruded void ratio (e_{HG}) and pore size density function ($\text{PSD} = -\Delta e_{\text{HG}}/\Delta(\log D)$) as a function of the

Table 1 Characteristics of tested specimens

| Test ID | Initial characteristics | | | Stresses before shearing | | Characteristics at equalization | | | Characteristics at failure | | |
|---------|----------------------------|--------------------------------|---|--|-------------------------|---------------------------------|-----------------------------|--------------------------------------|----------------------------|-----------------------------|--------------------------------------|
| | Void ratio e_0 (–) | Water ratio e_{w0} (–) | Degree of saturation S_{r0} (–) | Mean net stress p_{net} (kPa) | Suction s (kPa) | Void ratio e (–) | Water ratio e_w (–) | Degree of saturation S_r (–) | Void ratio e (–) | Water ratio e_w (–) | Degree of saturation S_r (–) |
| A1 | 0.550 | 0.420 | 0.77 | 50 | 50 | 0.644 | 0.573 | 0.89 | 0.631 | 0.583 | 0.92 |
| A2 | 0.564 | 0.403 | 0.71 | 50 | 100 | 0.648 | 0.564 | 0.87 | 0.620 | 0.572 | 0.92 |
| A3 | 0.568 | 0.411 | 0.72 | 50 | 200 | 0.642 | 0.552 | 0.86 | 0.634 | 0.544 | 0.86 |
| A4 | 0.548 | 0.414 | 0.75 | 100 | 50 | 0.624 | 0.562 | 0.90 | 0.603 | 0.573 | 0.95 |
| A5 | 0.568 | 0.414 | 0.72 | 100 | 100 | 0.634 | 0.552 | 0.87 | 0.595 | 0.545 | 0.92 |
| A5* | | | | 200 | 100 | 0.592 | 0.546 | 0.92 | 0.552 | 0.542 | 0.98 |
| A6 | 0.542 | 0.408 | 0.74 | 100 | 200 | 0.620 | 0.523 | 0.84 | 0.598 | 0.517 | 0.86 |
| A6* | | | | 200 | 200 | 0.594 | 0.512 | 0.86 | 0.574 | 0.508 | 0.88 |
| A7 | 0.550 | 0.425 | 0.78 | 200 | 50 | 0.567 | 0.560 | 0.99 | 0.541 | 0.539 | 1.00 |
| A8 | 0.543 | 0.420 | 0.77 | 50 | 500 | 0.553 | 0.459 | 0.83 | 0.549 | 0.453 | 0.82 |
| B1 | 0.542 | 0.414 | 0.77 | 50 | 0 | 0.649 | 0.649 | 1.00 | 0.651 | 0.651 | 1.00 |
| B2 | 0.568 | 0.425 | 0.75 | 100 | 0 | 0.642 | 0.642 | 1.00 | 0.610 | 0.610 | 1.00 |
| B3 | 0.550 | 0.406 | 0.73 | 200 | 0 | 0.586 | 0.586 | 1.00 | 0.541 | 0.541 | 1.00 |
| B4 | 0.586 | 0.420 | 0.72 | 300 | 0 | 0.554 | 0.554 | 1.00 | 0.510 | 0.510 | 1.00 |

* Refers to the second applied failure stage

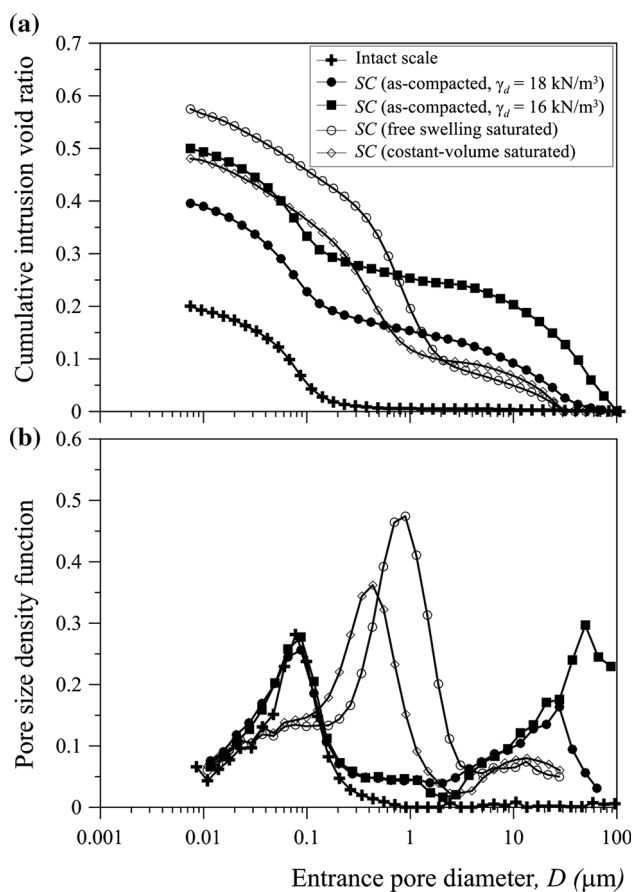


Fig. 1 Cumulative intruded void ratio (a) and pore size density function (b) on intact scale, as-compacted samples ($\gamma_d = 16\text{--}18 \text{ kN/m}^3$) and samples saturated after compaction

entrance pore diameter (D). Tested specimens include an intact stiff clay fragment (scale), as-compacted specimens at two different dry unit weights (equal to 16 and 18 kN/m^3) and specimens saturated after compaction in free and constrained conditions. Collected data analysis shows that the structure at microscopic level of as-compacted unsaturated scaly clay presents a clear double porosity network where two main levels of porosity are identified: the largest pores (macropores) can be associated with the inter-assembly porosity between assemblies composed of scaly fragments and clay aggregates, while the lowest pores (micropores, $d < 1 \mu\text{m}$) are located inside particle assemblies (intra-assembly porosity). Pore volume reduction induced by increased compaction energy, at the same water content, derives only from the inter-assembly pore volume reduction, while intruded volume and PSD function of the intra-assembly pores remain constant. The prevalent macropore entrance diameters decrease from 50 to 30 μm as γ_d increases from 16 to 18 kN/m^3 , while the prevalent micropore diameter coincides with the prevalent pore diameter (0.09 μm) of the intact scale. Besides, only minor

differences are detected between intruded volume and PSD distribution in the micropore domain of compacted material and intact stiff clay scale. There is clear evidence that the microstructure of the as-compacted unsaturated scaly clay depends mainly on the microstructure of intact stiff clay fragments (scales) that survive irrespective of the intensity of compaction stress.

The PSD of the specimen compacted to $\gamma_d = 16 \text{ kN/m}^3$ would suggest that inter-assembly pores larger than 100 μm exist, which are not detectable by the MIP technique.

Saturation modifies the structure of as-compacted scaly clay. Starting from the clear bimodal pore size distribution of the as-compacted clay specimen ($\gamma_{d,0} = 18 \text{ kN/m}^3$), saturation leads to a prevalent monomodal pore size distribution by means of swelling of assemblies and reduction in the inter-assembly pore volume. As a consequence, intra-assembly and inter-assembly pores are not distinguishable and the single-pore mode can be assigned to one or other group of pores. So, the dominant peak of the PSD function, determined by MIP after wetting in free swelling conditions, can be assumed as reference diameter to separate micro- and macropore domains [25]. This pore entrance diameter is assumed equal to $d = 1 \mu\text{m}$, very close to the prevalent monomodal pore diameter $d = 0.91 \mu\text{m}$ of the free swelling saturated sample. Swelling of assemblies depends on mechanical boundary conditions; the characteristic monomodal pore diameter of constant volume saturated samples (swelling pressure equal to 200 kPa) is significantly lower (0.45 μm) than the one observed in free swelling conditions.

The observation of the SEM photomicrograph of Fig. 2a highlights the structure of the as-compacted clay, characterized by large assemblies and macrovoids between them. Micropores inside aggregates are not easily discernible at photomicrograph magnification. Effects of saturation are well evident in the SEM photomicrograph of Fig. 2b: scale fragments and particle aggregations formed during compaction strongly expand invading the macrovoids. Expanded aggregates are arranged in a very uniform pattern with macrovoids ($d = 5\text{--}30 \mu\text{m}$) between them. However, scale fragments are still discernible as distinct units.

To quantify the evolution of the microstructure of compacted clay upon suction changes, Romero et al. [25] proposed a linear evolution of the microstructural void ratio e_m (accounting for intra-assembly porosity) with the amount of water stored in the material (expressed as the water ratio, e_w , the ratio of the volume of water to the volume of solid):

$$e_m = e_m^* + \beta \times (e_w - e_m^*) \quad \text{for } e_w > e_m^* \quad (1)$$

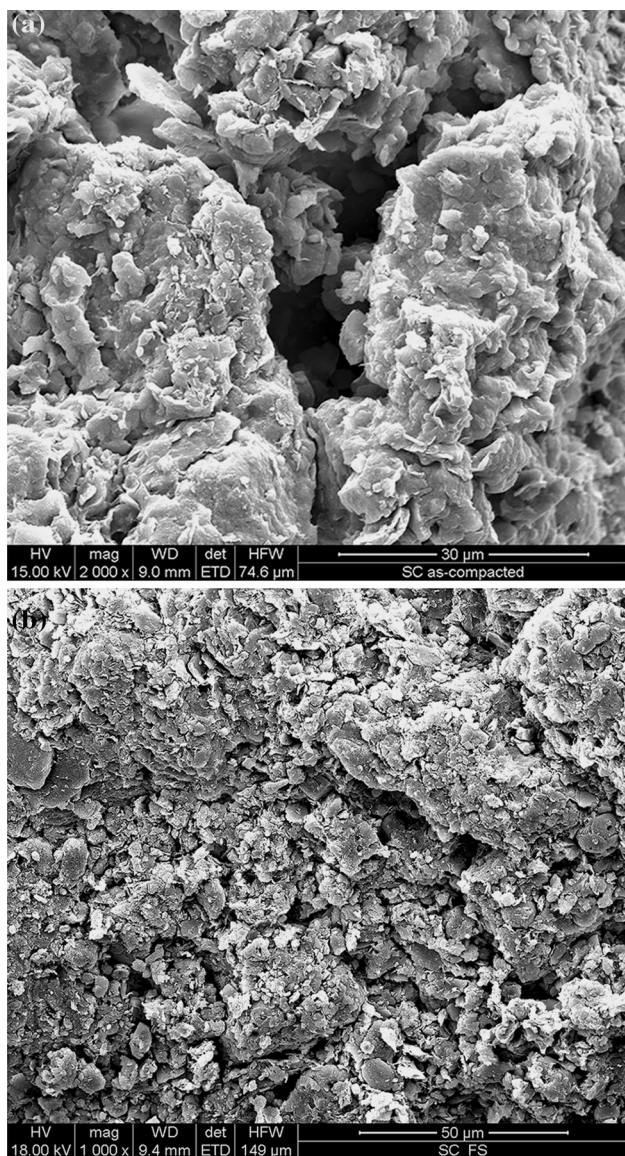


Fig. 2 SEM photomicrographs on freeze-dried samples: **a** as-compacted scaly clay $\gamma_d = 18 \text{ kN/m}^3$; **b** compacted scaly clay saturated under free swelling conditions

where the parameter β accounts for the swelling tendency of the assemblages and e_m^* represents the intra-assemblage void ratio corresponding to saturated micropores and empty macropores. When the water ratio is higher than e_m^* , water is starting to fill the macropores and the micropores start to swell significantly. This approach is used here to quantify the swelling potential of the assemblages resulting from the compaction of the scaly clay. In this sense, the results of MIP tests are plotted in Fig. 3, after calculation of the microstructural void ratio on the base of intruded void ratio in the range of diameter lower than $1 \mu\text{m}$; in the same plot, data from an ESEM microphotography campaign to quantify the swelling/shrinkage behaviour of scaly

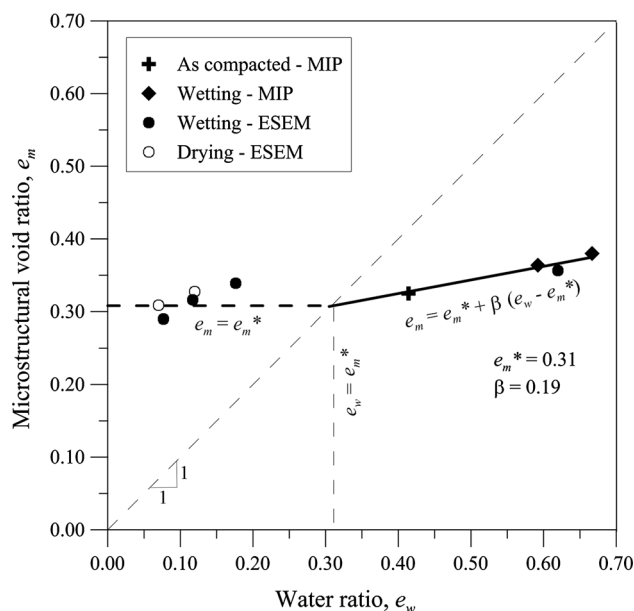


Fig. 3 Evolution of microporosity void ratio with water ratio from MIP and ESEM results

clay assemblages are also reported [13]. In this campaign, a clay aggregate was selected and subjected to suction-controlled wetting/drying cycles by modifying relative humidity and temperature in the ESEM chamber and the induced volumetric behaviour was monitored.

For every image, corresponding to an equalization stage along the imposed suction paths, aggregate areal deformation ϵ_{2D} was calculated relating the change in area with the initial area of the aggregate. The volumetric strain ϵ_v of the aggregate at the different wetting and drying equalization stages was quantified by means of the expression introduced by Romero and Simms [26] in order to take into account isotropic straining in the direction perpendicular to the image plane in which ϵ_{2D} was determined. The data are plotted in Fig. 3 converting suction into water ratio by means of the main wetting and main drying retention curves of the compacted clay [1], and calculating corresponding microstructural void ratio values on the base of volumetric strain and the initial void ratio, $e_{m0} = 0.29$. This last value was determined on an intact scale fragment, equalized at the same total suction applied at the beginning of the experiment in the ESEM chamber [3].

With reference to Eq. (1), data represented in Fig. 3 suggest a value of $e_m^* = 0.31$ and an interpolating slope $\beta = 0.19$ to calculate the evolution of the intra-assemblage void ratio at increasing water ratio in the domain $e_w > e_m^*$. The value of e_m^* is very close to the microstructural void ratio $e_m = 0.30$ of the as-compacted scaly clay that can be obtained by analysing the water retention curves in terms of water ratio e_w versus suction at constant void ratio equal to $e = 0.55, 0.60$ and 0.65 (Fig. 4). The retention curves in

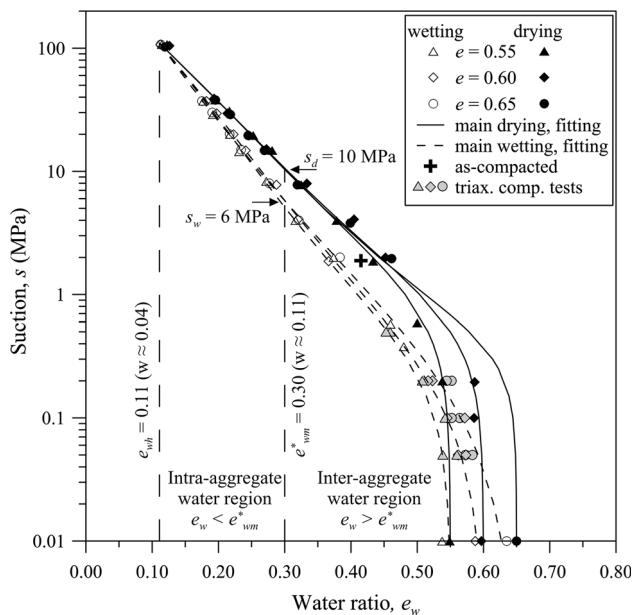


Fig. 4 Water retention curves for constant void ratio values equal to $e = 0.55\text{--}0.65$

Fig. 4 were obtained by least squares fitting of data representative of equalization conditions of samples subjected to main wetting and main drying paths, by using a modified form of the van Genuchten's type [27]. For each of the selected void ratios, only experimental data relative to samples with void ratio differing ± 0.025 from the considered one were fitted [1]. In Fig. 4, points representative of equalization and failure conditions of the samples subjected to the triaxial tests referred in the paper are also indicated.

Analysis of water retention curves suggests that the water ratio $e_w = 0.30$ can be assumed to subdivide the plots in two regions in which a different evolution of main retention curves with void ratio can be observed. For water ratio lower than 0.30, independent of the void ratio considered, water retention curves converge along two linear (semilog plot) envelopes related to drying and wetting paths, respectively, stemming from the point at hygroscopic water ratio (e_{wh}) (where drying paths end and wetting paths start). The two linear envelopes are very close but distinct. Suction values corresponding to e_w equal to $e_{wm}^* = 0.30$ are about 10 and 6 MPa, respectively, for the main drying and the main wetting retention curves. For water ratio values greater than 0.30, as void ratio increases main drying and main wetting retention curves move to the right and depart each other. This behaviour may be interpreted considering the double porosity features of the material structure.

Finally, it is not trivial to observe that the different values of e_{m}^* , determined by the different independent procedures outlined before, are in very good agreement.

4 Shear strength in unsaturated conditions

A comprehensive experimental programme was developed and executed with the aim to quantify suction effects on the shear strength of unsaturated compacted scaly clay. Suction-controlled triaxial compression tests on unsaturated samples and consolidated drained triaxial compression tests on saturated samples were carried out in order to investigate compacted clay shear strength in variable saturation conditions.

4.1 Experimental techniques and programme

Tests were carried out using a triaxial apparatus for testing unsaturated soil samples under controlled suction and stress path conditions [24]. The suction was controlled by means of the axis-translation technique: the required suction value was applied by setting constant pore air pressure (u_a) at the top base of the sample and varying water pressure (u_w) at the bottom of the sample through two different high air entry value porous discs (HAEV equal to 500 kPa and 1500 kPa).

Sample axial strains were calculated on the base of the piston axial displacements measured by means of a LVDT outside the cell. Radial strain values were obtained by monitoring water level variations in an inner cell coaxial to the sample [24]. A differential pressure transducer was used to measure the difference in water pressure between the base of the inner cell and that of a reference burette, with a resolution of ± 1 Pa ($\Delta \epsilon_r = 0.03\%$). A similar system connected to the water drainage line allowed us to measure water content variations.

The experimental programme was defined on the basis of two independent stress state variables, namely the mean net stress ($p_{net} = p - u_a$) and the matric suction ($u_a - u_w$), where p is the total mean stress [9, 15]. The shear strength of the unsaturated compacted scaly clay was investigated by isotropically consolidated drained suction-controlled triaxial compression tests in the range of confining net stress 50–200 kPa and matric suction in the range of 50–500 kPa.

Specimens were subjected to different isotropic hydro-mechanical stress paths before the deviatoric stage took place. In the first step, specimens were equalized at $p_{net} = 50$ kPa and $s = 50$ kPa. The equalization stage was considered completed when sample water content variations lower than 0.02 % per day were measured. Required time was in the range of about 700–800 h. Some of the samples were then dried at constant confining stress ($p_{net} = 50$ kPa) by increasing suction to $s = 100\text{--}200$ kPa. Isotropic compression to $p_{net} = 100\text{--}200$ kPa was carried out at constant suction. Specimen A8 was not subjected to the initial wetting step at $s = 50$ kPa, but it was equalized directly at $p_{net} = 50$ kPa and $s = 500$ kPa.

Because of the long time required by equalization in the wetting and drying stages, some tests (A4 \Rightarrow A4*, A5 \Rightarrow A5*, A6 \Rightarrow A6*) were carried out with a multistage technique, increasing confining net stress (from 100 to 200 kPa) at constant suction after a first deviatoric step. Specimen A7 was equalized to the same values used for the test A4* ($p_{\text{net}} = 200$ kPa and $s = 50$ kPa) and was sheared in order to evaluate the reliability of multistage test results. As shown in Fig. 5, where the tests A4* and A7 are compared, although initial stiffness is overestimated, the multistage technique, for the observed ductile behaviour, enables a reliable estimation of the failure conditions. For all tests, failure was achieved at constant suction in drained conditions (applied axial displacement rate equal to 0.028 mm/h). In order to verify that the displacement rate was appropriate to ensure the drained conditions, some preliminary experimental checks were carried out following the methodology proposed by Escario and Saez [12]. The deviatoric stage was halted for 80 h in order to allow dissipation of excess of water pressure, if any. Then, the test started again with the same rate verifying that the shear strength was not increased (Fig. 6).

Four complementary isotropic consolidated drained triaxial compression tests were carried out on saturated (back pressure $u_{w,0} = 400$ kPa) compacted scaly clay at confining effective stress of 50–300 kPa (series B in Table 1). All tests were performed at a constant temperature of 20 ± 1 °C.

4.2 Results of the controlled suction triaxial tests

In the initial equalization step, starting from the as-compacted condition ($e_{w0} = 0.42$, $\Psi_o \approx 2$ MPa), samples were wetted with imposed suction equal to $s = 50$ kPa and low isotropic stress ($p_{o,\text{net}} = 50$ kPa). Wetting followed main wetting retention curves with variable void ratio (Fig. 4), because the increase in water content at low confining pressure induced volumetric swelling equal to about $\varepsilon_v = 5$ –6 % and increased degree of saturation to

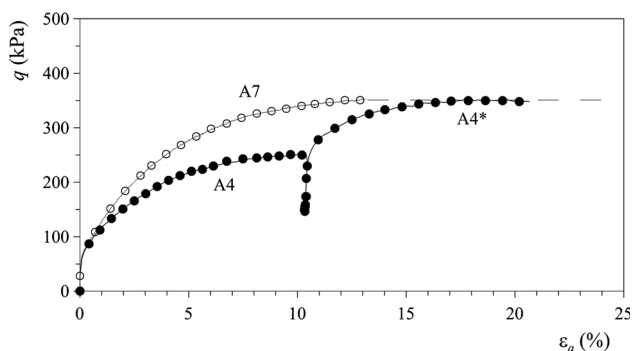


Fig. 5 Multistage test compared with single stage test

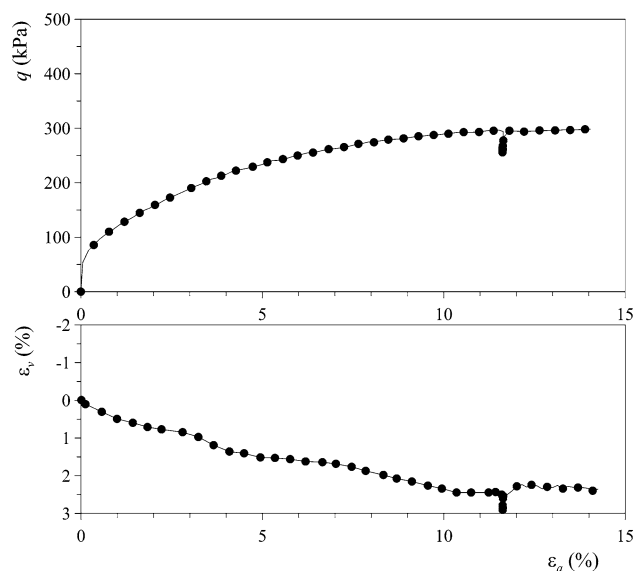


Fig. 6 Experimental verification of the adopted displacement rate

$S_r = 0.84$ – 0.89 . Successive drying at constant isotropic stress occurred at almost constant volume and water ratio, because of the moderate range of applied suction (50–200 kPa). Similarly, isotropic compression to $p_{\text{net}} = 100$ kPa did not induce any appreciable volumetric deformation or S_r variations for all applied suction values. However, in the A7 test, isotropic compression to $p_{\text{net}} = 200$ kPa ($s = 50$ kPa) produced a significant volumetric deformation ($\Delta\varepsilon_v \cong 3$ %) at an almost constant water content, increasing S_r to 0.99. Specimen A8 at the end of wetting at $s = 500$ kPa ($p_{o,\text{net}} = 50$ kPa) showed a moderate swelling ($\varepsilon_v \cong -0.6$ %) and a very low increase in water content and degree of saturation.

Values of void ratio, water content (in terms of water ratio) and degree of saturation of the tested samples at the end of equalization steps and at failure are collected in Table 1. Points representing void and water ratios of tested samples at the end of equalization, isotropic compression and deviatoric steps, as shown in Fig. 4, collect on (or very near) the corresponding main wetting retention curves (with reference to the current void ratio) [1].

The diagrams in Figs. 7, 8, 9 and 10 show deviatoric stress ($q = \sigma_1 - \sigma_3$), volumetric deformation (ε_v) and macropore degree of saturation, defined as the volume of water inside the inter-aggregate pores over the macropore volume ($S_{rM} = \frac{e_w - e_m}{e - e_m}$), in function of axial deformation (ε_a) for matric suction equal to 50, 100, 200 kPa and 500, respectively. The stress–strain curves (q – ε_a) show a typical hardening behaviour with, generally, contractive volumetric behaviour upon shearing. For matric suction in the range $s = 50$ – 200 kPa, a maximum deviatoric stress was reached for axial deformation between 10 and 12 %,

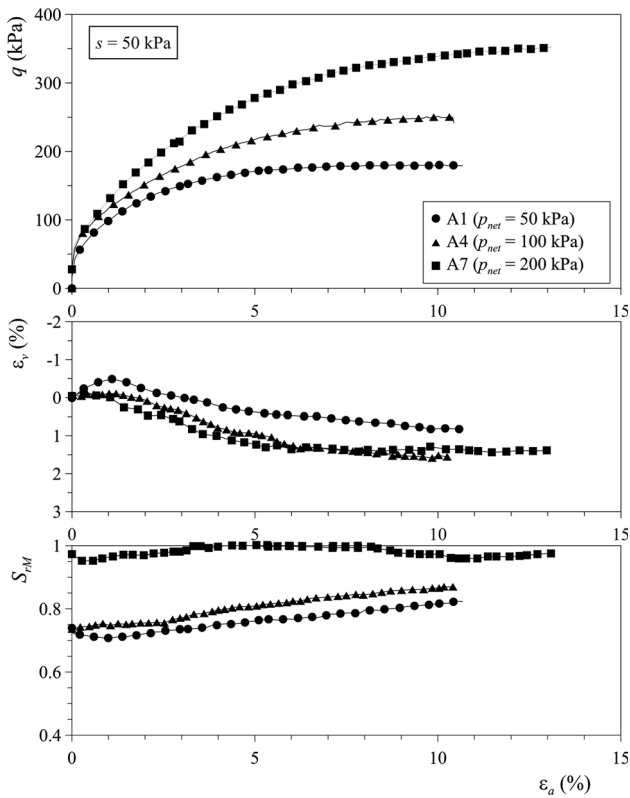


Fig. 7 Results of triaxial compression tests for $s = 50$ kPa

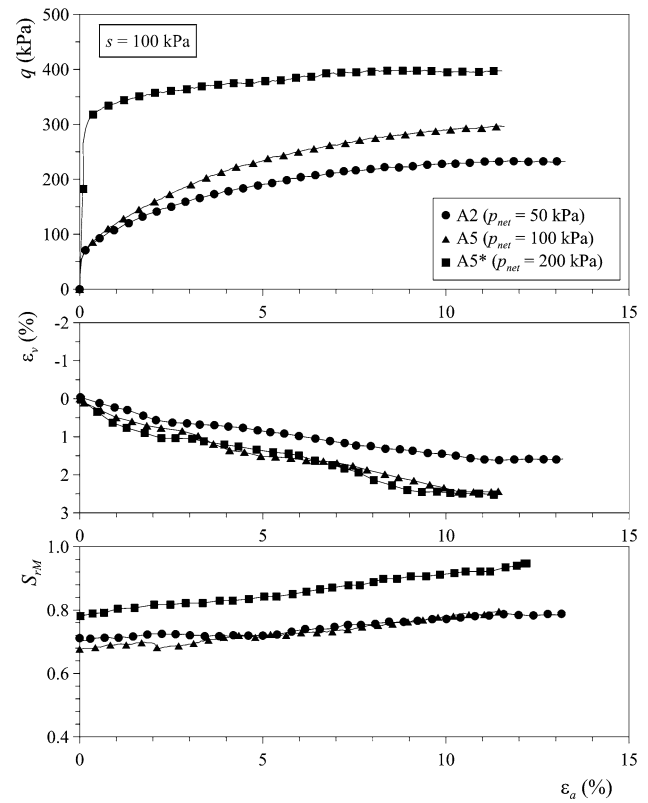


Fig. 8 Results of triaxial compression tests for $s = 100$ kPa

whereas for $s = 500$ kPa the sample A8 failed at axial deformation of about 6 %. High initial stiffness characterized samples tested with the multistage procedure (A4*, A5* and A6*), because of the unloading–reloading cycle of deviatoric stress necessary to increase the confining net stress, σ_{3net} , from 100 to 200 kPa.

In the failure steps, sample volumetric deformations were generally of compression type and in the range of 1–2.5 % for all applied suction values. An initial dilating behaviour, indeed of very low intensity ($\varepsilon_v \cong -0.5$ %), was observed at low stresses for suction equal to 50 kPa for sample A1 (Fig. 7), 200 kPa for samples A3, A6 (Fig. 9) and 500 kPa for samples A8 (Fig. 10). In this last case, however, volumetric deformations almost nil were observed for axial strain greater than 1 %.

An interpretation of the volumetric behaviour during the deviatoric loading phase can be provided by bearing on the concepts of the BExM [17], consistent with the double porosity network of the tested material. Effects of accumulated plastic volumetric strains on the loading collapse curve, LC, are shown in Fig. 11, which illustrates the calculated positions of the yielding locus in the plane ($\sigma_{v,net} - s$) as wetting and drying paths would be applied to the compacted scaly clay samples at a constant vertical net stress equal to $\sigma_{v,net} = 50$ kPa [28]. More precisely, the results depicted in Fig. 11 were obtained by modelling the

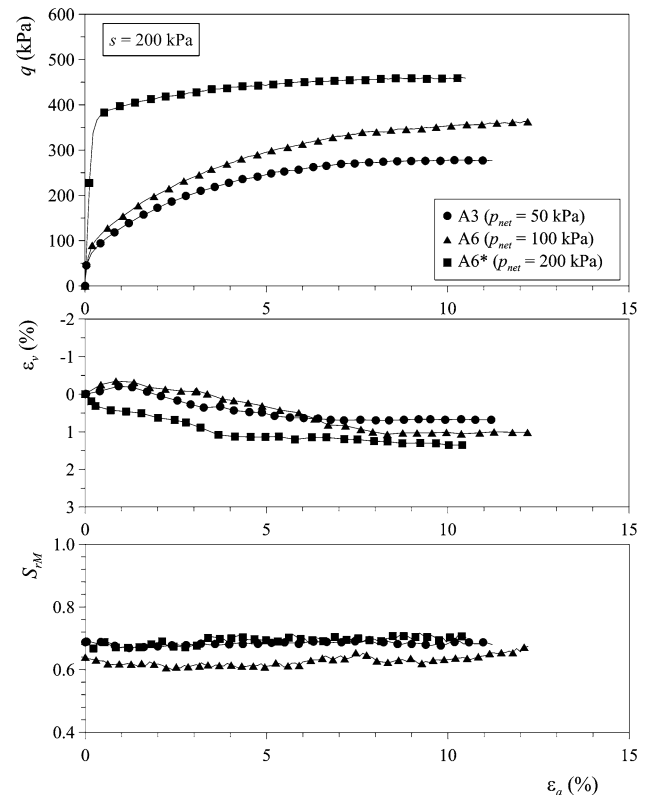


Fig. 9 Results of triaxial compression tests for $s = 200$ kPa

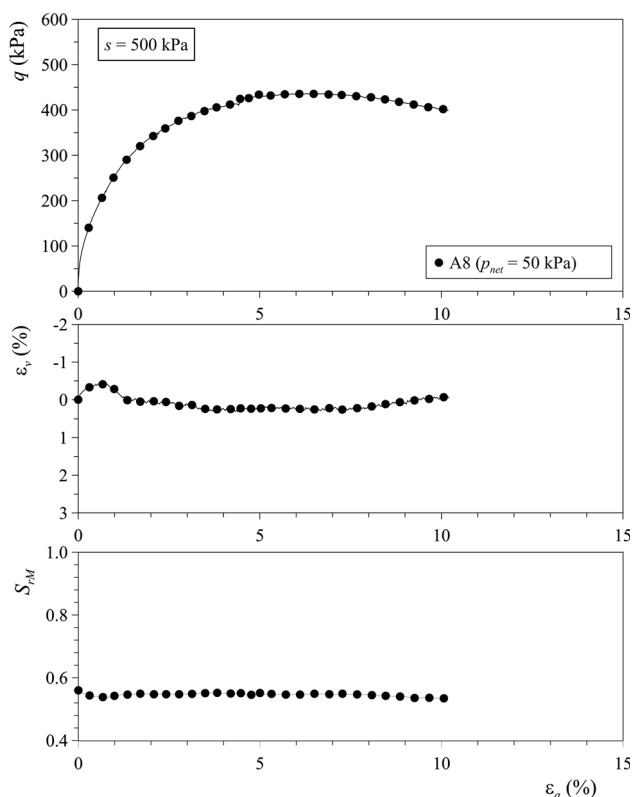


Fig. 10 Results of triaxial compression tests for $s = 500$ kPa

suction variation at constant vertical stress on compacted scaly samples having the same initial (preparation) properties of the triaxial test samples using the BExM model parameters derived by Airò Farulla et al. [3]. Although the simulation was carried out in oedometric conditions, results could be useful to highlight the behaviour of the material in the suction-controlled triaxial compression tests presented in this paper. Initial (equalization step) wetting at low confining pressure induces dominant plastic swelling strains that cause the LC locus to move to the left. The stress state at the end of the equalization step ($\sigma_{v,net} = 50$ kPa, $s = 50$ kPa), however, stays still at the left of the yield limit. LC curves of the samples subjected to the subsequent drying steps at $s = 100$ kPa and $s = 200$ kPa (only drying at $s = 200$ kPa is represented in Fig. 11) do not substantially move the LC curve to the right. As a consequence at the beginning of the loading steps, the stress points stay at a moderate distance on the left of the corresponding LC curves, that is, they share moderate OCR values. Indeed, the volumetric behaviour during shearing for those samples is of general moderate compression. In some cases, as for tests A1, A3 and A6 it possible to note very low swelling strains (lower or equal to 0.5 %) at the beginning of the deviatoric phase (ϵ_a in the order of 1 %) that, however, do not obscure the prevalent compressive sample behaviour.

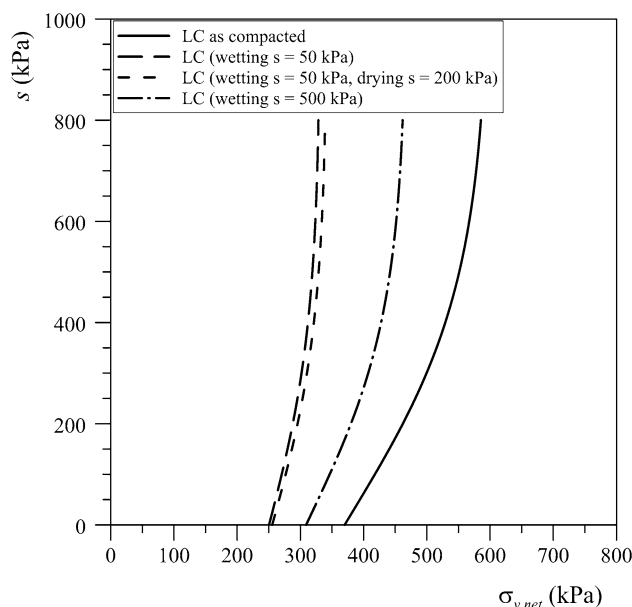


Fig. 11 Yielding curve in the as-compacted condition, after wetting at $s = 50$ kPa, after wetting at $s = 50$ kPa and successive drying stage at $s = 200$ kPa, after wetting at $s = 500$ kPa

In the case of test A8, swelling strains induced by wetting the sample at $s = 500$ kPa, as shown in Fig. 11, move the LC curve on the left in an intermediate position compared to the effects of equalization at $s = 50$ kPa. As a consequence, test A8, after an initial moderate swelling ($\epsilon_v \cong -0.4$ %), shows (Fig. 10) a stiff volumetric behaviour (very low volumetric deformations) due to the high applied suction ($s = 500$ kPa) or to the higher OCR (distance from LC curve), that, however, is not enough to induce a fully dilatant behaviour.

With reference to the water content variation during the deviatoric loadings, according to the approach later discussed, diagrams in Figs. 7, 8, 9 and 10 present the evolution of macropore degree of saturation versus axial strain, ϵ_a . The evolution of the macropore degree of saturation, S_{rM} , during the failure stage is affected by the applied suction. Except for the test on the specimen A7 that was nearly saturated at the beginning of the failure stage, S_{rM} increases for $s = 50$ and 100 kPa achieving values between 0.79 and 1.00; the corresponding total degree of saturation values is in the range $S_r = 0.92$ –1.00. For matric suction higher than the air entry value (~ 100 kPa), macropore degree of saturation retains almost constant values: for $s = 200$ kPa, it was in the range of 0.67–0.70, corresponding to a total degree of saturation equal to about 0.86, while for $s = 500$ kPa it was about 0.54, corresponding to a total degree of saturation equal to about 0.83.

The diagrams in Fig. 12 show deviatoric stress q and volumetric deformation as function of axial deformation ϵ_a for saturated samples. All the stress–strain curves (q – ϵ_a)

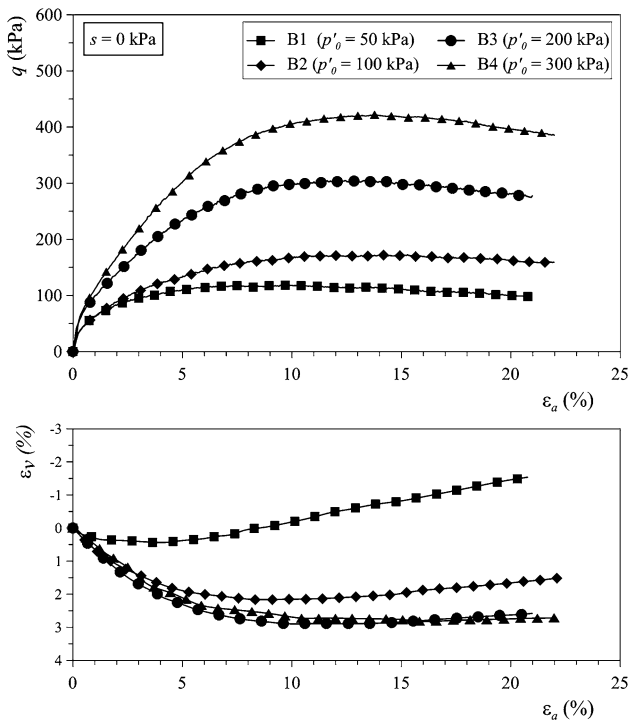


Fig. 12 Results of triaxial compression tests for saturated samples

show a typical hardening behaviour although at high deformation shear stress seems to be lightly decreasing. At the same time, the initial contractive behaviour changes into a dilatant one, very moderate for confining effective stress higher than 200 kPa.

Mohr circles at failure are shown in Fig. 13 for the different suction values, along with the circles related to saturated samples. The best fitting lines of each set of circles (least squares method) are characterized by shear strength angles ϕ' in the range of 20° – 22° and intercept cohesions increasing as suction increases.

According to the collected data, shear strength of the compacted scaly clay can be characterized by a shear strength angle ϕ' , which as first approximation can be considered constant, for both saturated and unsaturated samples and equal to 22° , and by an intercept cohesion c , which depends on applied suction. Shear strength envelope for $s = 500$ kPa was plotted assuming shear strength angles ϕ' equal to 22° .

In Fig. 14, intercept cohesion values c are fitted, in the range of the considered suction, by a hyperbolic envelope [16], having equation:

$$c = c' + s / (\cot\phi' + s/c^*) \tag{2}$$

where the saturated intercept cohesion c' is equal to 15 kPa and c^* is a fitting parameter (calculated by least squares method) equal to $c^* = 256$ kPa.

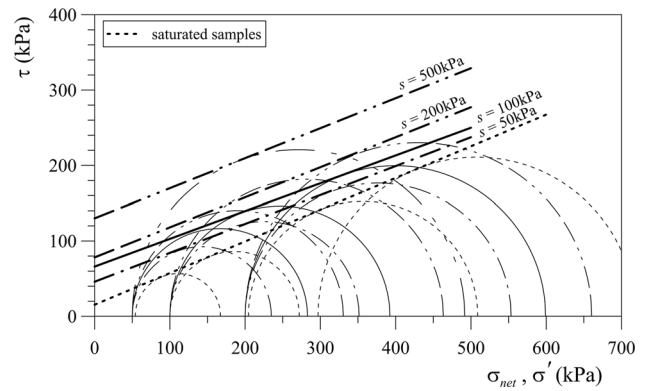


Fig. 13 Shear strength envelopes as a function of the applied matrix suction

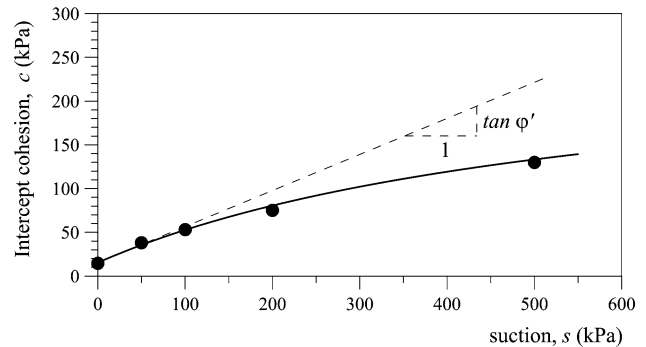


Fig. 14 Intercept cohesion values at increasing suction

For suction values lower or equal to 100 kPa, intercept cohesion values increase according to $\tan\phi'$, indicating that suction increments are equivalent to effective normal stress increments as in saturated soils. However, for $s = 200$ kPa, the increment of shear strength attenuates considerably. This observation agrees with the air entry value of compacted scaly clay samples, which is in the order of 100 kPa for void ratio $e = 0.55$ – 0.65 (Fig. 4).

5 Shear strength criterion in terms of effective stress

There is wide consensus in using an effective stress approach in order to interpret and model experimental data related to shear strength of unsaturated soils. Among the advantages of this approach, it is worth mentioning the smooth transition from saturated to unsaturated conditions and the possibility to evaluate shear strength of an unsaturated soil by using the parameters that characterize its behaviour when in a saturated state [10, 18, 20].

With reference to the effective stress, σ'_{ij} , derived from the initial Bishop's proposal by assuming the degree of saturation, S_r , for the χ parameter [10]:

$$\sigma'_{ij} = \sigma_{ij} - u_a \delta_{ij} + S_r(u_a - u_w) \times \delta_{ij}, \quad (3)$$

where δ_{ij} is Kronecker's delta, the failure criterion in the plane q, p' can be written as:

$$q = q_c + M \times [(p - u_a) + S_r(u_a - u_w)] \quad (4)$$

where q_c and M are, respectively, the intercept and the slope of the saturated envelope on the plane (q, p') .

It is known that in some circumstances the quantity $S_r(u_a - u_w)$ assumes unrealistic high values leading to erroneous evaluations in contrast with experimental data [10]. However, these evident shortcomings can be easily clarified and avoided considering the fundamental effects of microstructure characteristics on retention properties of unsaturated soils and their overall coupled hydro-mechanical behaviour [10, 27].

The question is very significant for compacted unsaturated high plasticity clays characterized, at microscopic level, by an aggregated structure with a double porosity network. As previously discussed, the double porosity affects deeply the water retention features of these materials, owing to the different retention mechanisms operating within micropores and macropores, respectively [27]. At high suction values, or low water contents, when water is present in the micropores and macropores are dry, void ratio changes, mainly due to a variation in macropore volume, do not induce any variation in retention properties. Adsorption mechanisms depend on mineralogical clay properties such as specific surface and plasticity.

At low suction values, when water content is high enough to partly fill the inter-assembly voids and to form menisci at assembly contacts, the dominant mechanism of water storage in the macropores is capillarity [29].

Analysis of the compacted scaly clay retention curves reported in Fig. 4 suggested that the water ratio $e_w = 0.30$ (corresponding to $w = 11\%$) can be assumed to distinguish regions in which the two different evolutions of main retention properties with void ratio can be observed. When the water ratio is higher than e_m^* , the macroporosity degree of saturation, S_{rM} , is higher than zero and water is starting to fill macropores. Capillary mechanism is dependent on prevalent macropore entrance diameters that are linked with the void ratio. Menisci, formed at assembly contacts, mechanically act as a skeleton stress governing stiffness and shear strength of the aggregated material. According to this point of view, capillarity or suction effects should be considered linked only to the amount of water partially filling the macropores. This observation seems well applicable to the case of scaly clays in which the shear strength behaviour is highly influenced by the mutual interactions among the scales.

In order to consider in an appropriate way the effects of suction on the shear strength of the unsaturated scaly clay,

the effective stress formulation reported in Eq. (3) has to be modified taking into account only the macropore degree of saturation as follows:

$$\sigma'_{ij} = \sigma_{ij} - u_a \delta_{ij} + S_{rM}(u_a - u_w) \times \delta_{ij} \quad (5)$$

Therefore, a shear strength criterion for unsaturated double structure soil can be defined as:

$$\begin{aligned} q &= q_c + (p_{net} + s \times S_{rM}) \times M \\ &= q_c + \left(p_{net} + s \frac{e_w - e_m}{e - e_m} \right) \times M \end{aligned} \quad (6)$$

where q_c and M are, respectively, the intercept and the slope of the saturated envelope on the plane (q, p') . This relation is similar to the one suggested by Tarantino and Tombolato [30]. However, the new proposal takes into account the interaction between the two main porosity networks, considering micropore volume variations when calculating macropore degree of saturation. To this aim, in order to evaluate the evolution of the saturated intra-aggregate pore volume when water ratio is higher than e_m^* , the linear relationship between e_m and e_w reported in Eq. (1) and depicted in Fig. 3 can be used.

Diagrams in Fig. 15 represent the stress paths of the triaxial compression tests on unsaturated and saturated compacted scaly clay obtained by representing measured deviatoric stress q values versus mean effective stress p' values, calculated according to the definition:

$$p' = (p - u_a) + s \frac{e_w - e_m}{e - e_m}. \quad (7)$$

Because macropore degree of saturation presents very low variations during drained compression, for the range of

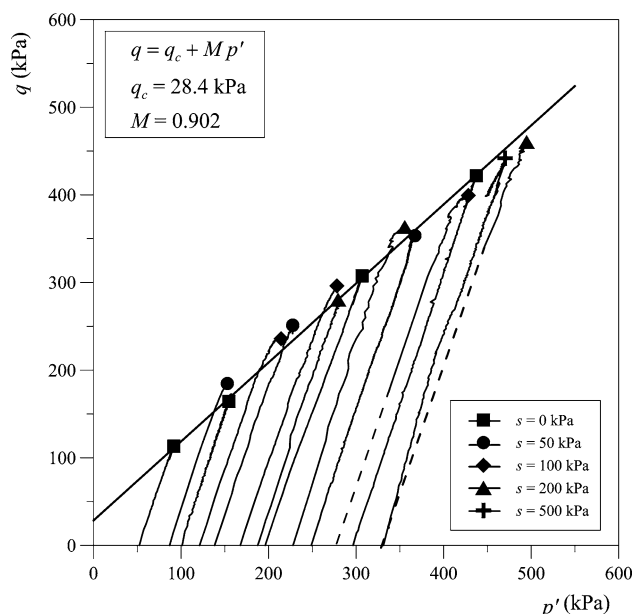


Fig. 15 Stress paths on the plane (p', q) of triaxial compression test

applied matric suction values, stress paths relative to the unsaturated compression tests are approximately linear with slope $(\delta q/\delta p')$ close to 3. As evident from Fig. 15, stress paths of unsaturated tests terminate, with only minor scatters, on the same failure envelope recovered from triaxial tests on saturated samples. Parameters of this unique failure envelope are as follows: $q_c = 28.4$ kPa and $M = 0.902$.

In order to stress the importance of considering the macropore degree of saturation when using a shear strength criterion in terms of effective stress for unsaturated soils, failure stress points are computed with Eq. (7) and plotted in Fig. 16 for three alternative choices of the Bishop’s parameter χ ; the points were obtained assuming χ equal to: (i) the evolving macropore degree of saturation (calculated by assuming $\beta = 0.19$, as it was the case in Fig. 3), (ii) a constant macropore degree of saturation ($e_m = 0.31$, $\beta = 0$) and (iii) the total degree of saturation.

Data represented in Fig. 16 highlight that the best representation is obtained when the macropore degree of saturation is used and the evolution of the microstructural void ratio is taken into account. The fitting is still good also when a constant microstructural void ratio is assumed and clearly unsatisfactory, especially for higher suction values, when the total degree of saturation is considered.

The choice of macropore degree of saturation as Bishop’s parameter χ is very effective to consider the most relevant aspects of suction influence on the shear strength of double porosity unsaturated soils. To this aim, considering the shear strength angle constant as applied suction varies, values of intercept cohesion $c = c' + s S_{rM} \tan \phi'$

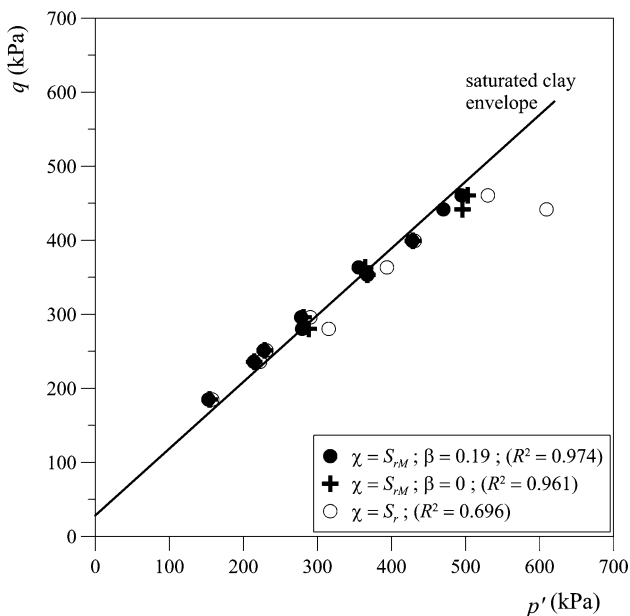


Fig. 16 Failure stress points for different definition of Bishop’s parameter

(where c' is the intercept cohesion of the saturated envelope) in the full range (1–0) of the macropore degree of saturation, S_{rM} , for constant void ratio values (0.55–0.65) are calculated and represented in Fig. 17. As suction increases (or S_{rM} decreases), c initially increases, reaches a maximum value and then decreases. When macropores are empty and S_{rM} becomes equal to zero, c , obviously, is again equal to intercept cohesion of saturated envelope c' . From the mathematical point of view, fitting curves are of polynomial type. However, for suction values in the order of some hundreds of kPa, as shown in Figs. 14 and 18, experimental data and calculated c values can be fitted very well by segment of hyperbola. As shown in Fig. 17, at equal suction values, c values in drying paths are greater than corresponding value in wetting paths; c values also increase as void ratio e decreases. The proposed approach could be very significant in modelling the behaviour of double porosity unsaturated soils subjected to generalized

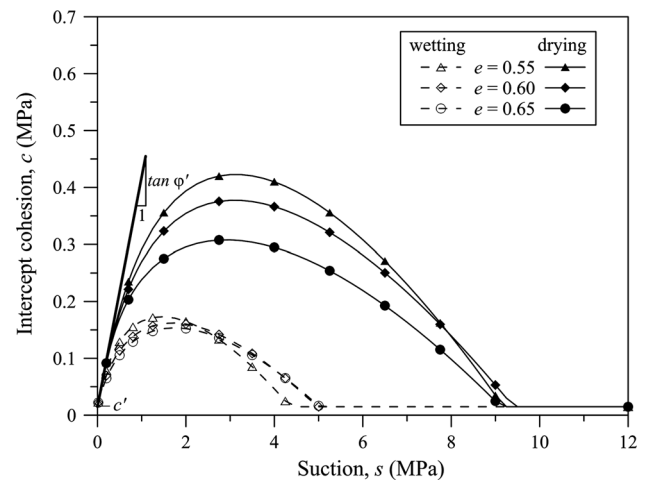


Fig. 17 Intercept cohesion modelled considering the macropore degree of saturation

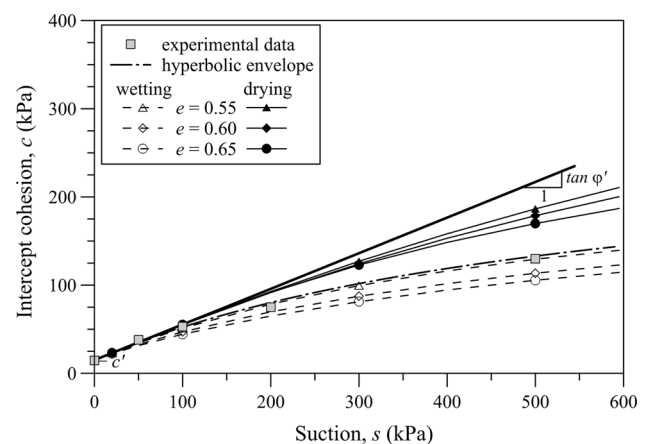


Fig. 18 Hyperbolic envelopes of intercept cohesion modelled considering the macropore degree of saturation in the range of suction $s = 0\text{--}600$ kPa

stress paths with high intensity suction variations as in the case of highly variable environmental conditions.

6 Conclusion

The paper presents results from an experimental campaign aimed at analysing the shear strength of a compacted, unsaturated scaly clay. Results of the triaxial tests carried out on saturated and unsaturated samples give further support to the suitability of effective stress approach in analysing shear strength behaviour of unsaturated compacted clays. In fact, it has been shown that points representative of failure conditions, expressed in terms of effective stresses, depict a unique failure envelope for both saturated and unsaturated samples. However, for compacted double-structured clays, a proper choice for the quantification of the water stored into the material is a crucial component to define the shear strength criterion. It has been shown that the best representation is obtained when the macropore degree of saturation is used in the definition of the effective stress and its evolution with the suction is taken into account. Indeed, the use of the macropore degree of saturation as Bishop's parameter χ permits to define the evolution of the intercept cohesion as a function of suction. According to this approach, cohesion vanishes when the interaction of menisci, formed at assemblage contacts, disappears due to the desaturation of the macropores. Furthermore, hydraulic hysteresis induces, at the same suction, different contribution to the shear strength. From a practical point of view, the microstructural void ratio and hence the macropore degree of saturation can be obtained in a quite straightforward way by porosimetry analysis of the as-compacted state. The determination of its evolution with suction (or water ratio) requires instead a more elaborated testing campaign. However, for the tested compacted clay, a satisfactory correlation can be achieved according to a simpler approach which assumes an invariant micropore void ratio. This assumption may not apply to clays with higher activity.

References

- Airò Farulla C, Battiato A, Ferrari A (2010) On the void ratio dependency of the retention behaviour for a compacted clay. In: Alonso E, Gens A (eds) Proceedings of the fifth international conference on unsaturated soils, vol 1. Taylor & Francis Group, London, pp 417–422
- Airò Farulla C, Ferrari A, Romero E (2007) Mechanical behaviour of compacted scaly clay during cyclic controlled-suction testing. In: Schanz T (ed) Experimental unsaturated soil mechanics. Springer proceedings in physics, vol 112. Springer, Berlin, pp 345–354. doi:10.1007/3-540-69873-6_35
- Airò Farulla C, Ferrari A, Romero E (2010) Volume change behaviour of a compacted scaly clay during cyclic suction changes. *Can Geotech J* 47(6):688–703. doi:10.1139/T09-138
- Airò Farulla C, Jommi C (2005) Suction controlled wetting-drying cycles on a compacted scaly clay. In: Bilsen H, Nalbatoğlu Z (eds) Proceedings of international conference on problematic soils, vol 1. Eastern Mediterranean University, Famagusta, N. Cyprus. 25–27 May 2005, pp 229–238
- Airò Farulla C, Nocilla N (1984) Assetto strutturale e resistenza di campioni di argilla a scaglie. *Rivista Italiana di Geotecnica* 3:148–157
- Airò Farulla C, Rosone M (2011) Microstructure and mechanical behaviour of a saturated compacted scaly clay. Paper presented at the proceedings of the XV European conference on soil mechanics and geotechnical engineering. Geotechnics of hard soils—weak rocks. ISSMGE, Athens, Greece, 12–15 September 2011
- Airò Farulla C, Rosone M (2012) Microstructure characteristics of unsaturated compacted scaly clay. In: Mancuso C, Jommi C, D'Onza F (eds) Unsaturated soils: research and applications. Springer, Berlin, pp 123–130. doi:10.1007/978-3-642-31116-1_16
- Airò Farulla C, Valore C (1993) Some aspects of the mechanical behaviour of compacted tectonized clays. Paper presented at the proceedings of an international symposium on geotechnical engineering of hard soils—soft rocks, Athens, Greece, 20–23 September 1993
- Alonso E, Gens A, Josa A (1990) A constitutive model for partially saturated soils. *Géotechnique* 40(3):405–430. doi:10.1680/geot.1990.40.3.405
- Alonso EE, Pereira J, Vaunat J, Olivella S (2010) A microstructurally based effective stress for unsaturated soils. *Géotechnique* 60:913–925
- Cardoso R, Romero E, Lima A, Ferrari A (2007) A comparative study of soil suction measurement using two different high-range psychrometers. In: Schanz T (ed) Experimental unsaturated soil mechanics, vol 112., Springer proceedings in physics Springer, Berlin, pp 79–93. doi:10.1007/3-540-69873-6_8
- Escario V, Saez J (1987) Shear strength of partly saturated soils versus suction. Paper presented at the proceedings of the 6th international conference on expansive soils, New Delhi
- Ferrari A (2007) Caratterizzazione meccanica di un'argilla a scaglie compattata non satura: effetti della suzione sulla resistenza al taglio. Ph.D. thesis, Università Mediterranea di Reggio Calabria, Università degli Studi di Palermo, Italy
- Ferrari A, Airò Farulla C, Romero E (2010) On the volumetric response of a compacted clay subjected to wetting and drying cycles. In: Unsaturated soils: theoretical and numerical advances in unsaturated soil mechanics—Proceedings of the 4th Asia Pacific conference on unsaturated soils, pp 89–94
- Fredlund D, Rahardjo H (1993) Soil mechanics for unsaturated soils. Wiley, New York
- Gens A (1993) Shear strength. In: Proceeding of unsaturated soils: recent developments and applications. Civil Engineering European Courses. UPC Barcelona, Spain, pp 1–13
- Gens A, Alonso E (1992) A framework for the behaviour of unsaturated expansive clays. *Can Geotech J* 29:1013–1032
- Jommi C (2000) Remarks on the constitutive modelling of unsaturated soils. In: Tarantino A, Mancuso C (eds) Experimental evidence and theoretical approaches in unsaturated soils. Balkema, Rotterdam, pp 139–153
- Koliji A, Vulliet L, Laloui L (2010) Structural characterization of unsaturated aggregated soil. *Can Geotech J* 47(3):297–311. doi:10.1139/T09-089
- Laloui L, Nuth M (2009) On the use of the generalised effective stress in the constitutive modelling of unsaturated soils. *Comput Geotech* 36(1–2):20–23

21. Leong EC, Tripathy S, Rahardjo H (2003) Total suction measurement of unsaturated soils with a device using the chilled-mirror dew-point technique. *Geotechnique* 53(2):173–182
22. Monroy R, Zdravkovic L, Ridley A (2010) Evolution of microstructure in compacted London Clay during wetting and loading. *Geotechnique* 60(2):105–119
23. Picarelli L, Di Maio C, Olivares L, Urciuoli G (1998) Properties and behaviour of tectonised clay shales in Italy. Paper presented at the Proceedings of the international symposium on the geotechnics of hard soils—soft rocks, Naples
24. Rampino C, Mancuso C, Vinale F (1999) Laboratory testing on an unsaturated soil: Equipment, procedures, and first experimental results. *Can Geotech J* 36(1):1–12
25. Romero E, Della Vecchia G, Jommi C (2011) An insight into the water retention properties of compacted clayey soils. *Geotechnique* 61(4):313–328
26. Romero E, Simms P (2008) Microstructure investigation in unsaturated soils: a review with special attention to contribution of mercury intrusion porosimetry and environmental scanning electron microscopy. *Geotech Geol Eng* 26:705–727
27. Romero E, Vaunat J (2000) Retention curves in deformable clays. In: Tarantino A, Mancuso C (eds) *Experimental evidence and theoretical approaches in unsaturated soils*. Proceedings of the international workshop on unsaturated soils, Trento. Balkema, Rotterdam, pp 91–106
28. Rosone M (2011) *Resistenza a taglio di un'argilla a scaglie compattata non satura*. Ph.D. thesis, Università Mediterranea di Reggio Calabria, Università degli Studi di Palermo, Italy
29. Salager S, Nuth M, Ferrari A, Laloui L (2013) Investigation into water retention behaviour of deformable soils. *Can Geotech J* 50(2):200–208
30. Tarantino A, Tombolato S (2005) Coupling of hydraulic and mechanical behaviour in unsaturated compacted clay. *Geotechnique* 55(4):307–317
31. Vitone C, Cotecchia F (2011) The influence of intense fissuring on the mechanical behaviour of clays. *Geotechnique* 61(12):1003–1018